Dalton Transactions

ROYAL SOCIETY OF CHEMISTRY

COMMUNICATION

View Article Online
View Journal | View Issue

Check for updates

Cite this: *Dalton Trans.*, 2025, **54**, 2252

Received 15th November 2024,
Accepted 10th December 2024

DOI: 10.1039/d4dt03207a

rsc.li/dalton

Dielectric properties depend on the crystal structure of perovskite-type $RbTaO_3$ synthesized at high pressure†

Kimitoshi Murase, [a] Jun-ichi Yamaura, [b] Yousuke Hamasaki, [c] Takeharu Kato, [d] Hajime Sagayama [e] and Ayako Yamamoto *[a]

We successfully synthesized perovskite-type $RbTaO_3$ at 1173 K under 4 GPa. $RbTaO_3$ crystalized as a cubic system (*Pm*$\bar{3}$*m* space group (SG), *a* = 4.04108(3) Å) at 300 K in contrast to the orthorhombic perovskite-type $RbNbO_3$ prepared under the same conditions. During the cooling process, it reversibly transformed into a tetragonal phase (SG: *P4mm*) at 270 K, and into an orthorhombic phase (SG: *Amm*2) at 80 K. Corresponding to the phase transition, the relative permittivity showed a peak at 270 K with a maximum value of approximately 2000 and a kink at 80 K. This transition scheme is analogous to well-known displacement-type ferroelectrics of $BaTiO_3$ and $KNbO_3$. This is in contrast to $KTaO_3$, which retains a cubic system and quantum paraelectric properties at the lowest temperature.

Displacement-type ferroelectrics with perovskite structures such as $BaTiO_3$,[1] $KNbO_3$,[2] and $PbTiO_3$ [3] have attracted attention in fundamental studies and applications. In recent decades, the performance has been nearly optimized in $BaTiO_3$, and a novel material is desired to achieve a breakthrough, particularly for lead-free ferroelectric. Once a high-performance compound is obtained, it will also be pristine for a piezoelectric instead of conventional Pb(Zr, Ti)O_3.[4]

Recently, perovskite-type $RbNbO_3$ [5] was synthesized from the non-perovskite-type ambient pressure phase (APP) of $RbNbO_3$ using a high-pressure technique. Rb^+ (coordination number (CN) = 12 and ionic radius (r_{Rb}) = 1.72 Å) was installed into the K^+ (CN = 12 and r_K = 1.64 Å)[6] site in perovskite-type $KNbO_3$ by the pressure effect. The structural phase transitions corresponding to temperature variation were investigated. Two tetragonal phases with c/a = 1.09 and 1.47 were found, and the coordination of Nb with O is octahedral and pyramidal. The spontaneous polarizations in the two tetragonal phases were estimated to be roughly 40 and 60 μC cm^{-2} based on the structures.[5] These values are comparable to 71 μC cm^{-2} in $LiNbO_3$.[7]

$KTaO_3$ is a well-known quantum paraelectric compound showing high dielectric permittivity ($\varepsilon_r \approx 4000$) at 10 K.[8] $KTaO_3$ has a cubic symmetry from below 5 K to 1600 K whereas $KNbO_3$ displays rhombohedral, orthorhombic, tetragonal, and cubic symmetries. Several findings indicate quantum paraelectric state breaks by element substitution[9,10] and external pressure.[11] The study of perovskite-type $RbTaO_3$ has only been reported theoretically with regard to its structural, electronic, optical, and thermoelectric properties, and the effect of pressure.[12–16] It would be highly significant to experimentally obtain perovskite-type $RbTaO_3$ and investigate the properties in comparison with the theoretical predictions.

In this study, we report the synthesis of perovskite-type $RbTaO_3$ (cubic: *Pm*$\bar{3}$*m* space group (SG), *a* = 4.04108(3) Å). It was obtained from a non-perovskite-type APP of $RbTaO_3$ (monoclinic SG: *C*2/*m*)[17,18] using a high-pressure technique. The ionic radii of Ta^{5+} and Nb^{5+} (CN = 6) provided by Shannon are the same[6] or that of Ta^{5+} is slightly bigger than Nb^{5+} according to the ionic radii calculated using machine learning.[19] However, experimentally the structural and dielectric properties of $RbTaO_3$ differ greatly from those of $RbNbO_3$, similar to the relationship between orthorhombic $KNbO_3$ and cubic $KTaO_3$. In $RbTaO_3$, we found three perovskite phases (orthorhombic 10–80 K, tetragonal 80–270 K, and cubic 270–972 K). The relative permittivity varied depending on the structure with a maximum value of *ca.* 2000 at 270 K in a bulk sample.

The synthesis of $RbTaO_3$ proceeded in two steps. The first step is the preparation of APP of $RbTaO_3$ from dried Rb_2CO_3 (Kojundo, 99%) and Ta_2O_5(Aldrich, 99.99%). The powders

[a]*Graduate School of Engineering and Science, Shibaura Institute of Technology, 307 Fukasaku, Minuma, Saitama, 337-8570, Japan. E-mail: ayako@shibaura-it.ac.jp*
[b]*Institute for Solid State Physics, University of Tokyo, Kashiwa, Chiba, 277-8581, Japan*
[c]*Department of Applied Physics, National Defence Academy, Yokosuka, Kanagawa, 239-8686, Japan*
[d]*Nanostructures Research Laboratory, Japan Fine Ceramics Center, 2-3-1 Mutsuno, Atsuta, Nagoya, 456-8587, Japan*
[e]*Institute of Materials Structure Science, High Energy Accelerator Research Organization, Tsukuba, Ibaraki 305-0801, Japan*
† Electronic supplementary information (ESI) available. See DOI: https://doi.org/10.1039/d4dt03207a

were weighed and mixed in a dry box, and sintered in air at 1173 K for 10 h. The second step involved high-pressure treatment. The APP was stuffed into a golden capsule and placed into the pressure medium with a heater and an insulator. It was heated at 1173 K for 30 min under 4 GPa using a 180-ton cubic anvil-type press (Try Eng. Co.), followed by a quick quench to room temperature.

Powder X-ray diffraction (XRD) was performed using a Bragg–Brentano diffractometer (SmartLab, Rigaku, Tokyo) with CuKα_1 radiation (λ = 1.5418 Å). Low-temperature XRD (SmartLab, Rigaku, Tokyo) was measured with CuKα_1 in the temperature range of 10–290 K. The transition temperature was also confirmed from Differential Scanning Calorimetry (DSC) measurements (Rigaku, DSCvesta2). Lattice parameters were determined using the whole powder pattern fitting method. For structural refinement, synchrotron powder XRD measurements were performed at room temperature at BL-8B (λ = 0.690388 Å) in the Photon Factory of KEK, Japan. The lab and synchrotron XRD patterns were analysed to determine the structural parameters using the Rietveld method with the software Z-Rietveld.[20] The sample's morphology was observed using scanning electron microscopy (SEM) (JCM-6000 NeoScope, JEOL). The chemical composition was confirmed by transmission electron microscopy (JEM-F200, JEOL Ltd, Tokyo) and electron microscopy–energy dispersive X-ray spectroscopy (EDS).

The dielectric properties were measured with a bulk disk (∅ 3.2 mm) using a precision inductance, capacitance, and resistance (LCR) meter (4284A; Agilent, Palo Alto, CA) at frequencies of 10^4–10^6 Hz in a temperature range of 4–298 K. Golden electrodes were applied by sputtering to both sides.

The XRD patterns of the APP and high-pressure phase (HPP) of $RbTaO_3$ changed drastically as seen in Fig. 1(a), indicating a structural phase transition from low to high symmetry. The pattern of HPP is almost identical to that of $KTaO_3$, although the peaks shifted to slightly lower angles. The SEM image is shown in Fig. S1.† EDX analysis of $RbTaO_3$ showed that the Rb : Ta ratio of 47.6 : 52.4 was close to stoichiometry. The process of obtaining a single phase of $RbTaO_3$ was not straightforward because of the high hydroscopic reactivity and high volatility of Rb. The single phase was obtained only by starting from a fully dehydrated APP. The details are illustrated in Fig. S2(a) and (b).† Fig. 1(b) and (c) display the obtained crystal structure of the APP and HPP. H_2O was easily captured between layers in the APP in an open atmosphere, while the HPP was dense and very stable once stabilised. We investigated the pressure threshold to stabilize perovskite-type $RbTaO_3$. It was obtained at 3 GPa, but not at 2 GPa. The density change from 6.331 g cm^{-3} to 7.911 g cm^{-3} represents a 23% reduction in volume, and it is comparable to that of $RbNbO_3$.[5]

The observed and calculated XRD patterns of the Rietveld analysis are shown in Fig. 1(d). The fitting appears reliable, and the refined structural parameters are listed in Table 1. The displacement parameter U of Rb is larger than that of Ta consistent with $KTaO_3$. The crystal structures of $RbTaO_3$ and $RbNbO_3$ are cubic and orthorhombic, respectively, at room temperature, although they were synthesized under the same high-pressure synthesis conditions.

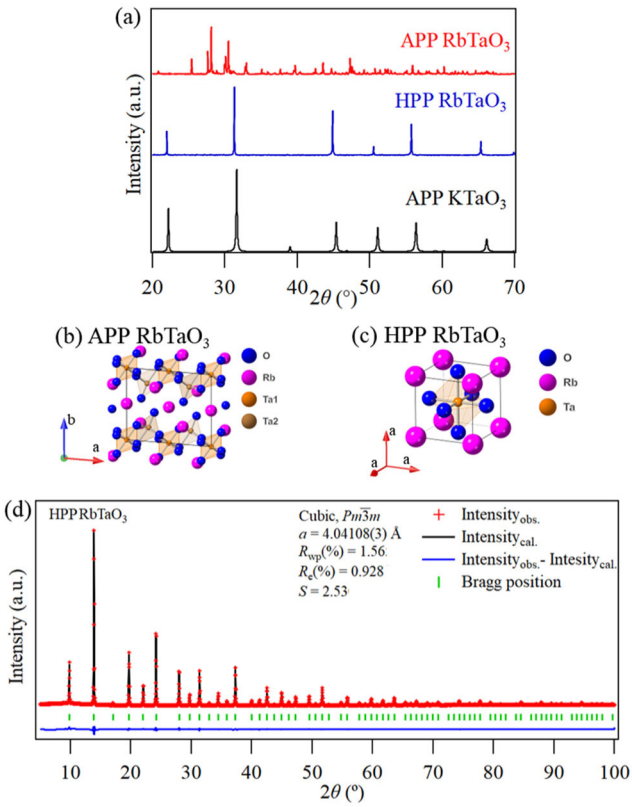

Fig. 1 (a) Powder XRD patterns (λ = 1.5418 Å) of the APP and HPP of $RbTaO_3$, and $KTaO_3$, (b) the crystal structure models of the APP of $RbTaO_3$, (c) the HPP of $RbTaO_3$, and (d) Rietveld analysis (λ = 0.690388 Å) of the HPP of $RbTaO_3$. R_{wp} = 1.57% and S = 2.53.

Table 1 Crystal structure information of the HPP of $RbTaO_3$. SG: $Pm\bar{3}m$ (cubic), and lattice parameters a and v were 4.04108(3) Å and 65.9924 (15) Å^3, respectively

Atom	Site	Occ.	x	y	z	U_{iso} (Å^2)
Rb	1a	1	0	0	0	0.00386(5)
Ta	1b	1	1/2	1/2	1/2	0.00244(4)
O	3c	1	1/2	0	1/2	0.00189(2)

Low-temperature XRD measurements revealed two phase transitions below room temperature at 270 K and 80 K. Fig. 2 shows powder XRD patterns in the wide and narrow ranges at 290–10 K.

The cooling process is depicted in Fig. 2(a-1), (a-2), and (a-3); a structural transition from the cubic to tetragonal phase at 270 K culminating in the tetragonal phase at 260 K is observed as shown in Fig. 2(a). Further transition to the orthorhombic phase started at 80 K, and finished at 70 K. No further phase transitions occurred down to 5 K, the lowest temperature we were able to detect. The sequential transitions were reversible, exhibiting a small temperature hyster-

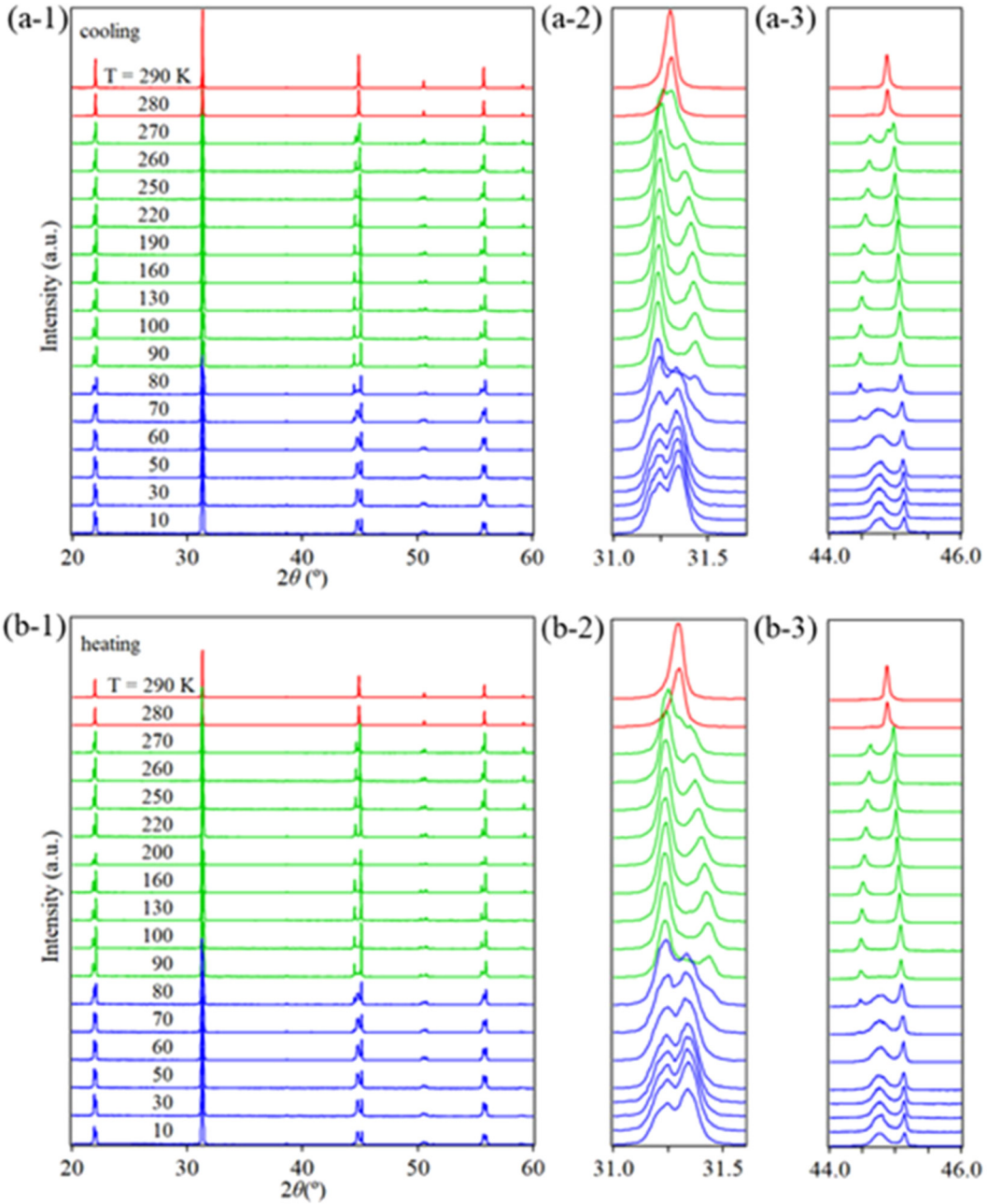

Fig. 2 Powder XRD patterns of the HPP of $RbTaO_3$ at 290–10 K (a) in the cooling process ((a-1) overall view, (a-2) 1 1 0 diffraction peak of the cubic phase, (a-3) 2 0 0 diffraction peak of the cubic phase) and (b) in the heating process, (b-1), (b-2) and (b-3) are same range. Red, green, and blue indicate cubic, tetragonal, and orthorhombic structures, respectively.

esis of less than 10 K. The transition sequences of $RbTaO_3$ are analogous to that of $KNbO_3$ and $BaTiO_3$ except for the appearance of the rhombohedral phase at lower temperatures. Fig. 3 shows the three polymorphisms of $RbTaO_3$ at the specific temperature. Structural analyses of the XRD patterns collected at 200 K and 10 K using the Rietveld method were performed; the same symmetry of transition was expected in $KNbO_3$. The c/a ratio of the tetragonal phase was 1.01 at 200 K, which is lower than that of $RbNbO_3$ and $KNbO_3$. Reasonable results were obtained, and the details are presented in Fig. S3(a) and (b).† The first transition temperature (cubic to tetragonal) and calorific value were also confirmed using DSC measurements. The transition temperature was 263.9 K on cooling and 270.2 K on heating. The details are provided in Fig. S4.†

Our *ab initio* calculations indicate that the orthorhombic phase is the most stable at the lowest temperature in $RbTaO_3$. The contract with $KTaO_3$ ensures a cubic phase at the lowest temperature owing to the suppression of structural transitions by quantum fluctuation.

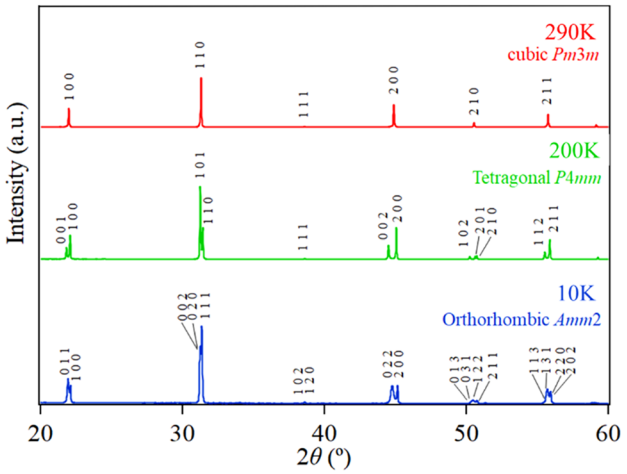

Fig. 3 XRD patterns and Miller indices of the three phases in the HPP of $RbTaO_3$.

The temperature dependence of the lattice parameters in the HPP of $RbTaO_3$ was plotted together with the relative permittivity (ε_r) in Fig. 4. As the temperature decreased, *a* shortened and *c* elongated until the transition to orthorhombic

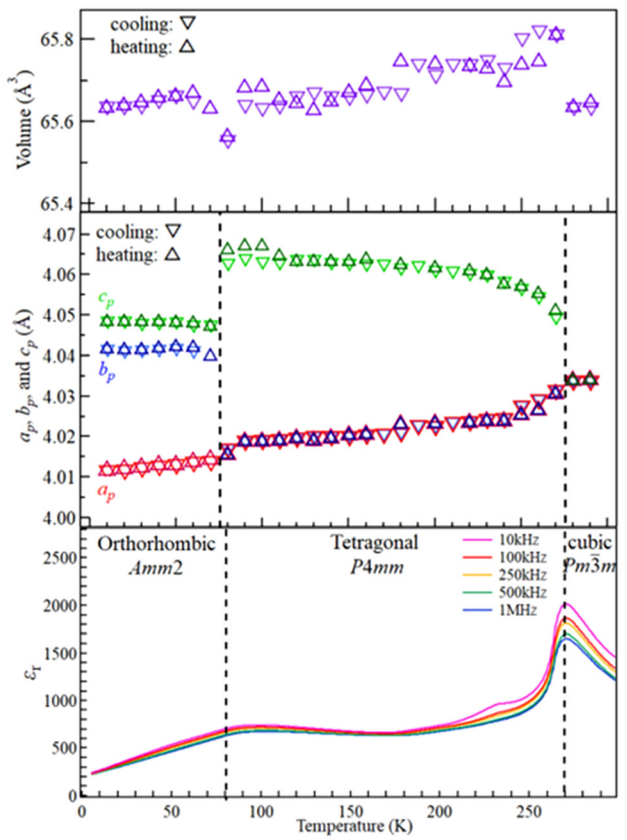

Fig. 4 Temperature dependence of lattice parameters, volume, and relative permittivity of a bulk disk, which has an 88% packing density, of $RbTaO_3$ at 4–280 K. a_p, b_p, c_p, and *v* are taken from a basic perovskite cell.

structure occurred. It appears unusual but a similar behaviour was observed in the temperature dependence of lattice parameters in $KNbO_3$.[2] In both cases, the volume monotonically decreased with decreasing temperature, indicating that the distortion becomes stronger at lower temperatures in the tetragonal phase. No substantial difference in the lattice parameters was observed between the cooling and heating processes. The volume increased slightly at the phase transition temperatures.

It is noted that the temperature dependence of ε_r corresponded exactly with that of the crystal structure as shown in Fig. 4. The ε_r at 1 MHz was *ca.* 1500 at 300 K, and showed a maximum of 1700 at 270 K, which was the temperature of cubic-tetragonal structural transition. It was constant at *ca.* 700 at 100–200 K in the tetragonal structure. A kink was observed at 80 K, corresponding to the tetra-*ortho* transition, and the ε_r was 200 at 5 K. This phenomenon is analogous to the known displacement-type ferroelectrics such as $BaTiO_3$ and $KNbO_3$ except for the appearance of the rhombohedral phase. In these ferroelectrics, ε_r showed a maximum at the tetra-cubic transition and was relatively flat in the tetragonal phase.

On the other hand, the structural behaviour of $RbTaO_3$ differs from those of $RbNbO_3$ and $KTaO_3$. Perovskite-type $RbNbO_3$ at 300 K crystallized in the orthorhombic phase; two tetragonal phases (Tetra1: c/a = 1.07 and Tetra2: c/a = 1.43) appeared with 670 K, and no cubic phase appeared. As revealed by high-temperature XRD, the cubic phase of $RbTaO_3$ was stable at 270–972 K and transformed into the APP as we will report elsewhere. This suggests structural distortion owing to size mismatch in the combination of Rb and Ta in the perovskite-type structure compared with that of Rb and Nb. The actual ionic size of Ta may be larger than that of Nb.

The quantum paraelectric state was not observed in $RbTaO_3$, unlike $KTaO_3$. This is probably because of a difference in the phonon distribution. Since only stoichiometric $KTaO_3$ is in the special situation the ferroelectric nature is suppressed by zero-point vibration, and this state is easily broken by pressure, strain, and substitution.[21]

In this work, we showed ε_r = 1500 (1 MHz), but a higher value of ε_r is expected in the higher density bulk or single crystal. If we could raise the Curie temperature above room temperature by substitution, $RbTaO_3$ would be a promising ferroelectric material. Perovskite-type $RbTaO_3$ has the potential for expansion of its promising ferroelectric properties; for example, we can stabilize the tetragonal phase.

Conclusions

Perovskite-type $RbTaO_3$ was obtained by the phase transition of non-perovskite $RbTaO_3$ at a high pressure of 4 GPa. The crystal system at 298 K is cubic ($Pm\bar{3}m$), the same as $KTaO_3$, but differs from orthorhombic $RbNbO_3$ prepared at high pressure. $RbTaO_3$ showed crystal structural transition from cubic to tetragonal phase at 270 K, and tetragonal to ortho-

rhombic phase at 80 K with decreasing temperature, while it returned to non-perovskite $RbTaO_3$ above 972 K. The dielectric properties of $RbTaO_3$ varied corresponding to the structural transition. Relative permittivity was 1100–1600 at room temperature and 10kHz to 1 MHz. The maximum relative permittivity, 1500–2000, was observed in the cubic to tetragonal phase transition. $RbTaO_3$ is a candidate for ferroelectrics including piezoelectrics near room temperature, although further investigation is needed to clarify the dielectric properties, *e.g.* a hysteresis loop. Partial substitution in Rb and Ta sites may induce a variation in the structural and ferroelectric properties.

Author contributions

Kimitoshi Murase: conceptualization, investigation, data curation, formal analysis, and writing – original draft and reviewing and editing. Junichi Yamaura: data curation and writing – review and editing. Yousuke Hamasaki: data curation and writing – review and editing. Takeharu Kato: data curation. Hajime Sagayama: data analysis. Ayako Yamamoto: conceptualization, investigation, formal analysis, and writing – review and editing.

Data availability

The data that support the findings of this study are available from the corresponding authors, Kimitoshi Murase and Ayako Yamamoto, upon reasonable request.

Conflicts of interest

There are no conflicts to declare.

Acknowledgements

This study was supported by the Innovative Science and Technology Initiative for Security grant number JPJ004596, ATLA, Japan. This study was also supported by the GRIMT program (202212-RDKGE-0018) at the Institute for Materials Research, Tohoku University, the Joint Research Program (202306-MCBXG-0079) at the Institute of Solid State Physics, University of Tokyo, and the approval of the Photon Factory Program Advisory Committee (Proposal No. 2024PF-Q001). Dr T. Kawamata and Dr K. Sugiyama of Tohoku University are thanked for the high-temperature XRD measurements. DSC measurements were performed by Rigaku. Co. (Tokyo). Some of the powder XRD measurements were performed at Technoplaza at Shibaura Institute of Technology.

References

1 M. Acosta, N. Novak, V. Rojas, S. Patel, R. Vaish, J. Koruza, G. A. Rossetti and J. Rödel, *Appl. Phys. Rev.*, 2017, **4**, 041305.
2 D. Wang, G. Wang, Z. Lu, Z. Al-Jlaihawi and A. Feteira, *Front. Mater.*, 2020, **7**, 91.
3 H. S. Bhatti, S. T. Hussain, F. A. Khan and S. Hussain, *Appl. Surf. Sci.*, 2016, **367**, 291–306.
4 T. R. Shrout and S. J. Zhang, *J. Electroceram.*, 2007, **19**, 113–126.
5 A. Yamamoto, K. Murase, T. Sato, K. Sugiyama, T. Kawamata, Y. Inaguma, J. Yamaura, K. Shitara, R. Yokoi and H. Moriwake, *Dalton Trans.*, 2024, **53**, 7044–7052.
6 R. D. Shannon, *Acta Crystallogr., Sect. A*, 1976, **32**, 751–767.
7 M. Minakata, *The Review of Laser Engineering (in Japanese)*, 2004, **32**, 175–180.
8 A. Tkach, P. M. Vilarinho and A. Almeida, *J. Eur. Ceram. Soc.*, 2011, **31**, 2303–2308.
9 J. G. Bednorz and K. A. Müller, *Phys. Rev. Lett.*, 1984, **52**, 2289–2292.
10 U. T. Höchli, H. E. Weibel and L. A. Boatner, *Phys. Rev. Lett.*, 1977, **39**, 1158–1161.
11 S. Triebwasser, *Phys. Rev.*, 1959, **114**, 63–70.
12 M. Sarwan and S. Singh, *Indian J. Phys.*, 2023, **97**, 2061–2076.
13 M. I. Hussain, R. M. Arif Khalil, F. Hussain, A. M. Rana, G. Murtaza and M. Imran, *Optik*, 2020, **219**, 165027.
14 M. Hassan, M. Liaqat and Q. Mahmood, *Appl. Phys. A*, 2021, **127**, 287.
15 M. Riaz, B. Ali, S. M. Ali, M. I. Khan, M. S. U. Sahar, M. Shahid and M. Alam, *J. Comput. Electron.*, 2024, **23**, 483–497.
16 A. I. Lebedev, *Phys. Solid State*, 2015, **57**, 331–336.
17 M. Serafin and R. Hoppe, *Z. Anorg. Allg. Chem.*, 1980, **464**, 240–254.
18 K. Fukuda, I. Nakai, Y. Ebina, R. Ma and T. Sasaki, *Inorg. Chem.*, 2007, **46**, 4787–4789.
19 A. A. B. Baloch, S. M. Alqahtani, F. Mumtaz, A. H. Muqaibel, S. N. Rashkeev and F. H. Alharbi, *Phys. Rev. Mater.*, 2021, **5**, 043804.
20 R. Oishi-Tomiyasu, M. Yonemura, T. Morishima, A. Hoshikawa, S. Torii, T. Ishigaki and T. Kamiyama, *J. Appl. Crystallogr.*, 2012, **45**, 299–308.
21 T. Esswein and N. A. Spaldin, *Phys. Rev. Res.*, 2022, **4**, 033020.

